Stator Resistance Estimation using DC Injection with Reduced Torque Ripple in Induction Motor Sensorless Drives

Jiwon Yoo, *Student Member, IEEE*, Joohyun Lee, *Student Member, IEEE*,
Seung-Ki Sul, *Fellow, IEEE*, and Noor Aamir Baloch.

***Abstract*— In this paper, the torque ripple of an induction motor due to dc injection for the stator resistance estimation is analyzed. In the analysis, the fundamental component of rotor flux is used for rotor flux orientation to avoid the perturbation issue in synchronous reference speed. On the synchronous reference frame, flux and torque fluctuation due to injected dc and arbitrary 2nd harmonic current is calculated. Furthermore, the current reference that nullifies the fundamental frequency torque ripple in the whole operating condition is proposed. An integral-based average filter is applied to extract dc signals in phase voltage and current. Simulations and experiments are carried out to verify the performance of the proposed methods.**

***Index Terms*— Induction motors, dc signal injection, sensorless control, stator resistance estimation, torque ripple reduction.**

NOMENCLATURE

$\mathbf{i}^{s}_{dqs} = \begin{bmatrix} i^{s}_{ds} \\ i^{s}_{qs} \end{bmatrix}$	Current vector at the stationary reference frame.
$\mathbf{i}^{\hat{e}}_{dqs} = \begin{bmatrix} i^{\hat{e}}_{ds} \\ i^{\hat{e}}_{qs} \end{bmatrix}$	Current vector at the estimated synchronous reference frame.
$\boldsymbol{\lambda}^{\hat{e}}_{dqr} = \begin{bmatrix} \lambda^{\hat{e}}_{dr} \\ \lambda^{\hat{e}}_{qr} \end{bmatrix}$	Rotor flux vector at the estimated synchronous reference frame.
$\Delta(\ )$	Ripple component.
$(\ )^{*}$	Reference value.
$\hat{(\ )}$	Estimated value.
R_s	Stator resistance.
R_r	Rotor resistance.
L_m	Magnetizing inductance.
σL_s	Stator transient inductance.
$\tau_r = L_m / R_r$	Rotor time constant.
ω_e	Synchronous speed.
ω_{sl}	Slip speed.

I. INTRODUCTION

THE estimation of stator resistance of an induction motor (IM) is important for improving stability and torque accuracy in sensorless control, and also can be used for thermal monitoring of the stator winding. Especially in sensorless drives, the accuracy of stator resistance information directly affects control performance in the low-speed region because the current model, which is an alternative to the voltage model, is not available in that region due to the lack of speed sensor [1]. Since the stator resistance varies considerably according to the load and environmental conditions, the online estimation method for the stator resistance is essential in sensorless drives not only to enhance control accuracy but also to keep the stability of the control system [2].

There are two main categories in the online estimation of the stator resistance. One is the methods using model reference adaptive system (MRAS), which exploit the rank redundancy of IM model equations [2]-[5]. On the other hand, the stator resistance also can be estimated by injecting dc in the stationary reference frame during operation [6]-[13]. If the dc injection method is applied, the rank redundancy of IM model could be used for other parameter estimation [14]-[16].

However, the application of dc injection method has been limited to the thermal monitoring, and it has not been applied for control purposes due to the large torque ripple from the injected current. When the only dc current is injected in the stationary reference frame, the synchronous *q*-axis current fluctuates and torque ripple occurs inevitably.

To mitigate this torque ripple, the additional 2nd order harmonic current injection method was proposed [6]-[8]. In [6] and [7], the 2nd order harmonic current nullifies the synchronous *q*-axis current ripple while maintains the magnitude of injected dc current. Thanks to the low-pass filtering effect by the rotor circuit of IM, the injected synchronous *d*-axis current induces little flux fluctuation in the mid- and high-speed region. Thus, the torque ripple could be significantly reduced in these speed regions compared to the case where only dc is injected.

However, the accuracy of stator resistance is crucial for control performance in the low-speed region, where the *d*-axis current fluctuation is not filtered sufficiently. The remaining *d*-axis current fluctuation causes large flux and torque ripples at low speed. In addition, this torque ripple would result in speed fluctuation, which makes sensorless control more difficult. Furthermore, the large flux ripple can cause the perturbation in synchronous speed in the low-speed region. The ripple in the synchronous speed can deteriorate the current control performance and the injection of dc current itself would also be distorted.

Instead of nullifying *q*-axis current ripple, a method of injecting dc and 2nd order harmonic current along the constant torque curve was proposed [8]. It can significantly reduce the torque ripple in the whole speed region. However, its applications are limited to the permanent-magnet synchronous motors (PMSMs), not IMs.

Since dc and 2nd order harmonic currents fluctuate on the

synchronous reference frame, the current regulator should provide the high bandwidth enough to control the fluctuating current without delay. To achieve this in the high-speed region, the proportional-resonant current controller has been adopted [9].

In dc injection, the extraction of dc signal is also important. Various extraction methods have been researched. To obtain precise phase voltage information from voltage reference, the compensation methods of the inverter non-linearity effect in dc signal injection were proposed [10], [11], instead of installing an additional voltage sensing circuit [9], [12]. To extract dc signal from phase voltage and current, notch/low-pass filter on the synchronous reference frame was used [9], [11]. Meanwhile, F. Baneira et al. [13] analyzed the synchronous speed fluctuation due to dc injection in low-inertia applications, and proposed dc signal extraction filter on the stationary reference frame.

However, most conventional dc extraction methods are not applicable in the low-speed region. In the low-speed region, the operating frequency components and dc signal are not separated enough in the frequency domain. Thus, the conventional dc extraction methods using frequency-based linear filters cannot sufficiently segregate the dc signal from the operating frequency components.

Unlike [6] and [7], which neglected the flux ripple due to the injected current, this paper analyzes the torque ripple considering the flux fluctuation generated by an arbitrary dc and 2nd harmonic current injection. Through the analysis, the optimal current injection trajectory minimizing the torque ripple due to the current injection is proposed. The proposed method is applicable for the whole operating condition and is effective, especially in the low-speed region. Besides, to inject dc as much as desired under large flux ripples, the fundamental flux-oriented control is proposed. Furthermore, the dc signal information is extracted using an angle-based synchronized filter, instead of the frequency-based linear filters [9], [11], [13], which are vulnerable to the low operating frequency. By reducing the torque ripple with the proposed methods, dc injection method can be applied to IM sensorless drive even in the low-speed region to improve torque accuracy and control stability without much penalty on torque ripple.

In addition to the previous work [17], this paper provides the following improvements.

1) Detailed mathematical analysis of the proposed method.
2) dc signal extraction method in the low-speed region.
3) Simulation and experimental results at various operating conditions.

II. DC AND 2ND HARMONIC CURRENT INJECTION

It is well known that the stator resistance can be estimated by injecting dc signal into IM [6]-[13]. When an additional current is injected into the motor, the current reference can be expressed as

$$\mathbf{i}_{\mathbf{dqs}}^{\hat{e}\,*} = \mathbf{I}_{\mathbf{dqs}}^{\hat{e}\,*} + \Delta\mathbf{i}_{\mathbf{dqs}}^{\hat{e}\,*}. \tag{1}$$

$\mathbf{I}_{\mathbf{dqs}}^{\hat{e}\,*}$ denotes the fundamental current at the estimated synchronous reference frame, which generates average flux and torque. $\Delta\mathbf{i}_{\mathbf{dqs}}^{\hat{e}}$ represents the injected current for stator resistance estimation at the estimated synchronous reference frame.

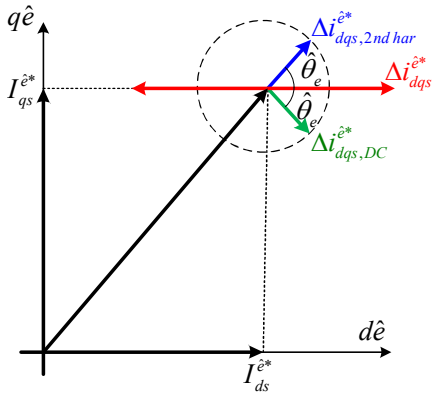

Fig. 1. Conventional dc and 2nd harmonic current injection.

When the dc current with the magnitude of $I_{DC\,Inj}{}^{*}$ is injected to the stationary d-axis, the injected current reference can be represented as

$$\Delta\mathbf{i}_{\mathbf{dqs}}^{\mathbf{s}\,*} = \begin{bmatrix} \Delta i_{ds}^{s\,*} \\ \Delta i_{qs}^{s\,*} \end{bmatrix} = \begin{bmatrix} I_{DC\,Inj}{}^{*} \\ 0 \end{bmatrix}. \tag{2}$$

By calculating the ratio between dc components of stationary d-axis voltage reference and injected current for one electrical period, T, the stator resistance can be estimated by

$$\hat{R}_s = \left(\tfrac{1}{T}\int_0^T v_{ds}^{s\,*}\,dt\right) \Big/ \left(\tfrac{1}{T}\int_0^T i_{ds}^{s\,*}\,dt\right). \tag{3}$$

Since the current is regulated on the estimated synchronous reference frame, the current reference in (2) can be converted to the one at the estimated synchronous reference frame as follows by multiplying the rotation matrix, $\mathbf{R}(-\hat{\theta}_e)$.

$$\Delta\mathbf{i}_{\mathbf{dqs}}^{\hat{\mathbf{e}}\,*} = \mathbf{R}(-\hat{\theta}_e)\cdot\Delta\mathbf{i}_{\mathbf{dqs}}^{\mathbf{s}\,*} = I_{DC\,Inj}{}^{*}\cdot\begin{bmatrix} \cos(\hat{\theta}_e) \\ -\sin(\hat{\theta}_e) \end{bmatrix}. \tag{4}$$

Injected current in (4) contains synchronous d- and q-axis injected currents, $\Delta i_{ds}^{\hat{e}\,*}$ and $\Delta i_{qs}^{\hat{e}\,*}$, which fluctuate with the synchronous speed, ω_e. In the high-speed region, $\Delta i_{ds}^{\hat{e}\,*}$ is filtered out through the rotor circuit of IM, and d-axis flux fluctuation, $\Delta\lambda_{dr}^{\hat{e}}$, can be neglected. However, in the low-speed region, $\Delta\lambda_{dr}^{\hat{e}}$ due to $\Delta i_{ds}^{\hat{e}\,*}$ has a non-negligible effect on vector control. If the conventional rotor flux-oriented vector control is applied, ω_e would also fluctuate [13]. This fluctuating synchronous frame deteriorates the current control performance, and actual injected current may differ from (4). Hence, this paper proposes fundamental rotor flux orientation (FRFO), which synchronizes the reference frame to the fundamental component of rotor flux. FRFO allows the synchronous speed to be kept as the average speed of rotating flux. The detailed implementation method for FRFO is described in chapter IV.

Meanwhile, the injected current in (4) can generate torque ripple in the whole operating region due to the torque

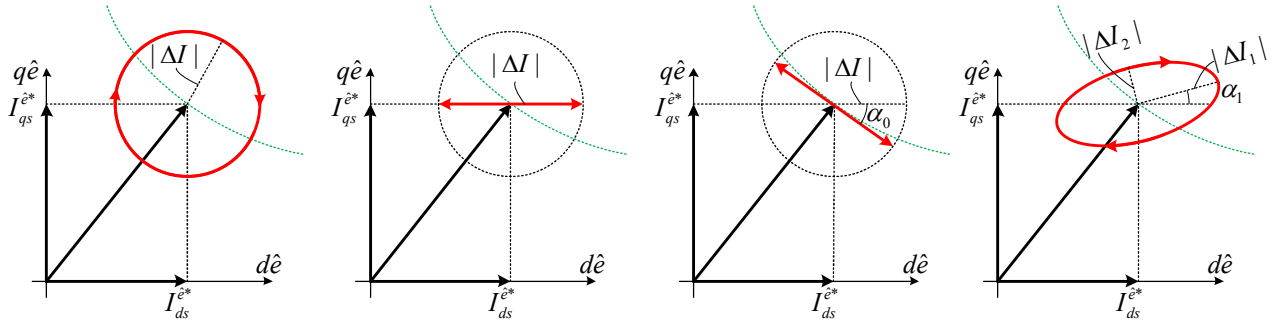

Fig. 2. Arbitrary dc and 2nd harmonic current injection.
(a) dc injection w/o 2nd harmonic. (b) *d*-axis injection (Conventional dc and 2nd harmonic injection). (c) Tilted axis injection. (d) Injection with tilted ellipse.

component current fluctuation, $\Delta i^{\hat{e}*}_{qs}$. Furthermore, $\Delta\lambda^{\hat{e}}_{dr}$ at low speed also generates torque ripple. To mitigate these torque ripples, dc and 2nd harmonic current injection methods have been proposed [6]-[7]. Both stationary dc and 2nd harmonic currents are expressed in terms of the fundamental frequency components on the synchronous reference frame, where dc is the negative sequence, and 2nd harmonic is the positive sequence. Therefore, a proper 2nd harmonic current injection can reduce the torque ripple due to the dc injection, while maintaining the magnitude of dc current. Ref. [7] injected 2nd harmonic current with the same magnitude of dc to nullify $\Delta i^{\hat{e}*}_{qs}$, as shown in Fig. 1. Then the current reference at the estimated synchronous reference frame can be derived as

$$\Delta\mathbf{i}^{\hat{e}*}_{\mathbf{dqs}} = \underbrace{I^{*}_{DC\,Inj}\begin{bmatrix}\cos(\hat{\theta}_e)\\ -\sin(\hat{\theta}_e)\end{bmatrix}}_{\text{DC injection}} + \underbrace{I^{*}_{DC\,Inj}\begin{bmatrix}\cos(\hat{\theta}_e)\\ \sin(\hat{\theta}_e)\end{bmatrix}}_{2^{\text{nd}}\text{ harmonic injection}}$$

$$= 2I^{*}_{DC\,Inj}\begin{bmatrix}\cos(\hat{\theta}_e)\\ 0\end{bmatrix}. \quad (5)$$

Because $\Delta i^{\hat{e}*}_{qs}$ is nullified and $\Delta i^{\hat{e}*}_{ds}$ does not cause $\Delta\lambda^{\hat{e}}_{dr}$ in the mid- and high-speed regions, torque ripple would be significantly reduced except for the low-speed region. In contrast, $\Delta i^{\hat{e}*}_{ds}$ is doubled compared to the dc injection in (4). Since $\Delta\lambda^{\hat{e}}_{dr}$ also would be doubled, still large torque ripple would be generated in the low-speed region.

In this paper, the current injection method minimizing the torque ripple is proposed. The flux and torque fluctuation due to dc and 2nd harmonic currents with arbitrary phase and magnitude are calculated, and the current reference minimizing the torque ripple is deduced.

A current reference including dc and arbitrary 2nd harmonic current can be represented as

$$\Delta\mathbf{i}^{\hat{e}*}_{\mathbf{dqs}} = \begin{bmatrix}\Delta I^{\hat{e}*}_{ds}\cos(\hat{\theta}_e-\beta_d)\\ \Delta I^{\hat{e}*}_{qs}\cos(\hat{\theta}_e-\beta_q)\end{bmatrix}. \quad (6)$$

As IM satisfies the symmetry regardless of current injection angle, *d*-axis injection phase offset, β_d, can be set to zero for simplicity without loss of generality. Then (6) can be rewritten as

$$\Delta\mathbf{i}^{\hat{e}*}_{\mathbf{dqs}} = \Delta\mathbf{I}^{\hat{e}*}_{\mathbf{dqs,cos}}\cos(\hat{\theta}_e) + \Delta\mathbf{I}^{\hat{e}*}_{\mathbf{dqs,sin}}\sin(\hat{\theta}_e) \quad (7)$$

where

$$\Delta\mathbf{I}^{\hat{e}*}_{\mathbf{dqs,cos}} = \begin{bmatrix}\Delta I^{\hat{e}*}_{ds}\\ \Delta I^{\hat{e}*}_{qs}\cos(\beta_q)\end{bmatrix}. \quad (8)$$

$$\Delta\mathbf{I}^{\hat{e}*}_{\mathbf{dqs,sin}} = \begin{bmatrix}0\\ \Delta I^{\hat{e}*}_{qs}\sin(\beta_q)\end{bmatrix}. \quad (9)$$

In (7), $\Delta\mathbf{I}^{\hat{e}*}_{\mathbf{dqs,cos}}$ and $\Delta\mathbf{I}^{\hat{e}*}_{\mathbf{dqs,sin}}$ are the magnitude of cosine and sine components on *d*- and *q*-axis at FRFO, respectively. Fig. 2(a)-(d) show various cases of dc and 2nd harmonic injection trajectory, and each case can be expressed with (7). For example, Fig. 2(a) is the dc current injection and can be expressed as

$$\begin{bmatrix}\Delta I^{\hat{e}*}_{ds}\\ \Delta I^{\hat{e}*}_{qs}\\ \beta_q\end{bmatrix} = \begin{bmatrix}|\Delta I|\\ |\Delta I|\\ -\pi/2\end{bmatrix}. \quad (10)$$

The conventional dc and 2nd harmonic current injection is shown in Fig. 2(b), which is the case where $\Delta i^{\hat{e}*}_{qs}$ is set to null. Likewise, when β_q is zero, the current injection forms a trajectory as in Fig. 2(c). Fig. 2(d) shows the most generalized case of arbitrary dc and 2nd harmonic current injection.

The magnitude of injected dc current and its torque ripple can be decided by the values of $\Delta i^{\hat{e}*}_{ds}$, $\Delta i^{\hat{e}*}_{qs}$, and β_q. The injected dc current at the stationary reference frame, $\mathbf{I}^{\mathbf{s}*}_{\mathbf{dqs,DC}}$, can be formulated as

$$\mathbf{I}^{\mathbf{s}*}_{\mathbf{dqs,DC}} = \frac{1}{2\pi}\int_0^{2\pi}\Delta\mathbf{i}^{\mathbf{s}*}_{\mathbf{dqs}}d\hat{\theta}_e = \frac{1}{2}\begin{bmatrix}\Delta I^{\hat{e}*}_{ds} - \Delta I^{\hat{e}*}_{qs}\sin(\beta_q)\\ \Delta I^{\hat{e}*}_{qs}\cos(\beta_q)\end{bmatrix}. \quad (11)$$

Meanwhile, a certain level of injected dc current should be guaranteed to secure enough signal-to-noise ratio (SNR) considering inverter non-linearity or sensing errors in voltage and current measurements. Therefore, in this paper, torque ripple is compared under the condition of the same magnitude of the injected dc current for fair comparison between various methods.

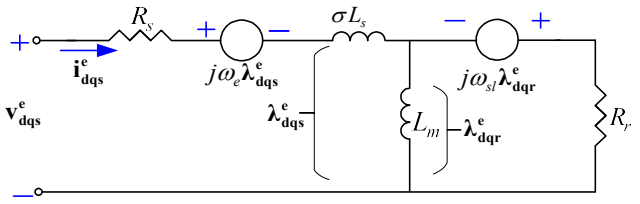

Fig. 3. Inverse-Γ model of IM

TABLE I. MOTOR PARAMETERS.

Rated power	3.7	kW
Rated frequency	60	Hz
Rated current	14	A_{rms}
Rated line to line voltage	220	V_{rms}
Stator resistance(R_s)	0.5	Ω
Mutual inductance(L_m)	60	mH
Rotor time constant(τ_r)	0.2	s

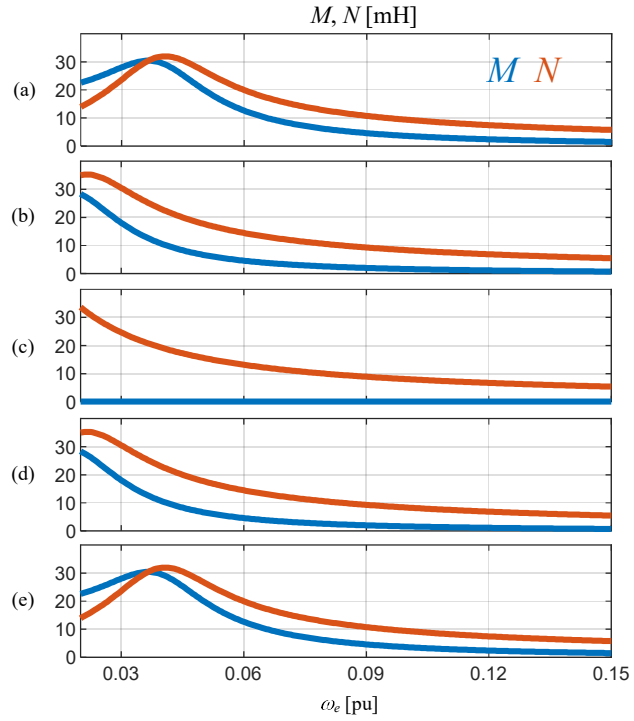

Fig. 4. Graph of M and N according to ω_e and T_e.
(a) T_e=−1.0 pu. (b) T_e =−0.5 pu. (c) T_e =0 pu. (d) T_e =0.5 pu. (e) T_e =1.0 pu.

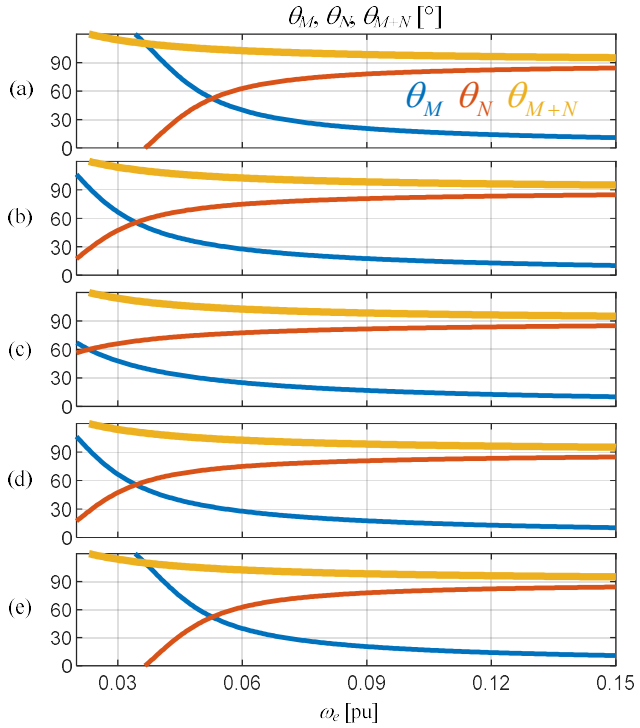

Fig. 5. Graph of θ_M, θ_N, and θ_{M+N} according to ω_e and T_e.
(a) T_e=−1.0 pu. (b) T_e =−0.5 pu. (c) T_e =0 pu. (d) T_e =0.5 pu. (e) T_e =1.0 pu.

III. R_S ESTIMATION WITH REDUCED TORQUE RIPPLE

A. Flux and Torque Ripple due to Current Injection

The inverse-Γ model of IM is shown in Fig. 3, and its rotor flux equation can be expressed as

$$\tau_r \frac{d}{dt}\boldsymbol{\lambda}^{\hat{e}}_{\mathbf{dqr}} = L_m \mathbf{i}^{\hat{e}}_{\mathbf{dqs}} - \left(\mathbf{I} + \mathbf{J}\tau_r\omega_{sl}\right)\boldsymbol{\lambda}^{\hat{e}}_{\mathbf{dqr}}. \quad (12)$$

In (12), τ_r stands for rotor time constant, L_m for magnetizing inductance, ω_{sl} for slip frequency, $\mathbf{I}$ for $\begin{bmatrix}1 & 0\\ 0 & 1\end{bmatrix}$, and $\mathbf{J}$ for $\begin{bmatrix}0 & -1\\ 1 & 0\end{bmatrix}$. If the current reference of (7) is injected, the differential equation (12) would result in the following form of the solution in the steady state.

$$\boldsymbol{\lambda}^{\hat{e}}_{\mathbf{dqr}} = \boldsymbol{\Lambda}^{\hat{e}}_{\mathbf{dqr}} + \Delta\boldsymbol{\Lambda}^{\hat{e}}_{\mathbf{dqr,cos}}\cos(\hat{\theta}_e) + \Delta\boldsymbol{\Lambda}^{\hat{e}}_{\mathbf{dqr,sin}}\sin(\hat{\theta}_e). \quad (13)$$

Eq. (13) can be segregated into three components; one for average flux, $\boldsymbol{\Lambda}^{\hat{e}}_{\mathbf{dqr}}$, one for a coefficient vector of cosine term, $\Delta\boldsymbol{\Lambda}^{\hat{e}}_{\mathbf{dqr,cos}}$, and one for a coefficient vector of sine term, $\Delta\boldsymbol{\Lambda}^{\hat{e}}_{\mathbf{dqr,sin}}$.

Since the steady state and FRFO are assumed, ω_e can be treated as constant and the following equation can be obtained.

$$\frac{d}{dt}\begin{bmatrix}\cos(\hat{\theta}_e)\\ \sin(\hat{\theta}_e)\end{bmatrix} = \begin{bmatrix}-\omega_e\sin(\hat{\theta}_e)\\ \omega_e\cos(\hat{\theta}_e)\end{bmatrix}. \quad (14)$$

Applying (13) and (14) to (12), the flux ripple, in the steady state, can be calculated as

$$\boldsymbol{\lambda}^{\hat{e}}_{\mathbf{dqr}} = \boldsymbol{\Lambda}^{\hat{e}}_{\mathbf{dqr}} + \Delta\boldsymbol{\lambda}^{\hat{e}}_{\mathbf{dqr}} = \begin{bmatrix}\Lambda^{\hat{e}}_{dr}\\ 0\end{bmatrix} + \begin{bmatrix}N\Delta I^{\hat{e}\,*}_{ds}\cos(\hat{\theta}_e - \theta_N)\\ M\Delta I^{\hat{e}\,*}_{ds}\cos(\hat{\theta}_e + \theta_M)\end{bmatrix} + \begin{bmatrix}-M\Delta I^{\hat{e}\,*}_{qs}\cos(\hat{\theta}_e - \beta_q + \theta_M)\\ N\Delta I^{\hat{e}\,*}_{qs}\cos(\hat{\theta}_e - \beta_q - \theta_N)\end{bmatrix} \quad (15)$$

where

$$M = L_m\frac{g}{\sqrt{\left(f^2-g^2+1\right)^2+4g^2}}. \quad (16)$$

$$N = L_m\frac{\sqrt{1+f^2}}{\sqrt{\left(f^2-g^2+1\right)^2+4g^2}}. \quad (17)$$

$$\tan\theta_M = \frac{2f}{f^2-g^2-1}. \quad (18)$$

$$\tan\theta_N = f\frac{f^2-g^2+1}{f^2+g^2+1}. \quad (19)$$

The detailed process to get (15)-(19) is described in APPENDIX. In (16)-(19), f stands for $\tau_r\omega_e$, and g for $\tau_r\omega_{sl}$. Therefore, f and g would correspond to operating speed and torque, respectively. The graphs of M, N, θ_M, and θ_N are shown in Fig. 4 and Fig. 5 for the IM with the nominal parameters listed in TABLE I. In Fig. 5, θ_{M+N} denotes $\theta_M+\theta_N$. M, N, θ_M, and θ_N have symmetry on the positive and negative ω_{sl}. N and θ_N are the self-inductance and its phase shift from $\Delta I_{ds}^{\hat{e}*}$ and $\Delta I_{qs}^{\hat{e}*}$ to $\Delta\Lambda_{dr}^{\hat{e}}$ and $\Delta\Lambda_{qr}^{\hat{e}}$, respectively. M and θ_M are the cross-coupling inductance and its phase shift from $\Delta I_{ds}^{\hat{e}*}$ and $\Delta I_{qs}^{\hat{e}*}$ to $\Delta\Lambda_{qr}^{\hat{e}}$ and $\Delta\Lambda_{dr}^{\hat{e}}$, respectively.

Observing (16), M is null when ω_{sl} is zero, and it can be noted that there is no cross-coupling term at the no-load condition. However, even if there is an only d-axis current injection in the loaded condition, both d- and q-axis fluxes would fluctuate because of the presence of M. Besides, since M and N converge to null as ω_e increases, the flux ripple due to current injection decreases as the speed increases.

Based on the calculated flux in (15) and the current reference in (7), the output torque can be calculated as follows:

$$T_e\left(\hat{\theta}_e\right) = \frac{3P}{4}\left(\lambda_{dr}^{\hat{e}}i_{qs}^{\hat{e}} - \lambda_{qr}^{\hat{e}}i_{ds}^{\hat{e}}\right) = T_{e,avg} + \Delta T_{e,\omega_e} + \Delta T_{e,2\omega_e} \quad (20)$$

where

$$T_{e,avg} = \frac{3P}{4}\Lambda_{dr}^{\hat{e}}I_{qs}^{\hat{e}*}. \quad (21)$$

$$\Delta T_{e,\omega_e}\left(\hat{\theta}_e\right) = \frac{3P}{4}\left(\Delta\lambda_{dr}^{\hat{e}}I_{qs}^{\hat{e}*} + \Lambda_{dr}^{\hat{e}}\Delta i_{qs}^{\hat{e}} - \Delta\lambda_{qr}^{\hat{e}}I_{ds}^{\hat{e}*}\right). \quad (22)$$

$$\Delta T_{e,2\omega_e}\left(\hat{\theta}_e\right) = \frac{3P}{4}\left(\Delta\lambda_{dr}^{\hat{e}}\Delta i_{qs}^{\hat{e}} - \Delta\lambda_{qr}^{\hat{e}}\Delta i_{ds}^{\hat{e}}\right). \quad (23)$$

$T_{e,avg}$ stands for the average torque, $\Delta T_{e,\omega e}$ for the torque ripple fluctuating with ω_e, and $\Delta T_{e,2\omega e}$ for that fluctuating with 2nd harmonic frequency, $2\omega_e$. $\Delta T_{e,2\omega e}$ consists of the products of the ripple variables, and $\Delta T_{e,\omega e}$ comes from the product of an average variable and a ripple variable. Since the flux and current ripples are smaller than their average values, $\Delta T_{e,\omega e} >> \Delta T_{e,2\omega e}$ can be satisfied.

B. Torque Ripple in Conventional Methods

The torque ripples in conventional methods can be calculated from (20)-(23). For dc injection method (conventional method 1) and conventional dc and 2nd harmonic injection method (conventional method 2), the magnitudes of $\Delta T_{e,\omega e}$ can be deduced as (24) and (25).

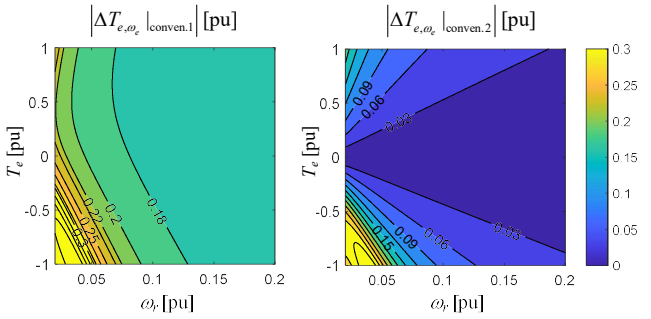

Fig. 6. Torque ripple in conventional methods.
(a) Conventional method 1. (b) Conventional method 2.

The approximations in (24) and (25) are based on the property of θ_{M+N}, which is

$$\theta_{M+N} = \text{atan2}(f,-1) \approx \pi/2 \quad (26)$$

where $f = \tau_r\omega_e >> 1$. Fig. 6(a) and (b) demonstrates the calculated torque ripples in conventional method 1 and 2 according to rotor speed and output torque when the injected dc current is 0.1 pu, respectively. As shown in (24) and Fig. 6(a), $L_m I_{ds}^{\hat{e}*} I_{DC\,Inj}^{\ *}$ remains even in the mid-speed region and the torque ripple does not decrease in conventional method 1. In the case of conventional method 2, the torque ripple converges to zero in the mid-speed region, as shown in (25) and Fig. 6(b). However, in the low-speed region, torque ripple does not vanish at the loaded conditions, where $M \neq 0$ and $I_{qs}^{\hat{e}*} \neq 0$.

C. Proposed Current Injection Method

$\Delta T_{e,\omega e}$ can be nullified by selecting proper $\Delta I_{ds}^{\hat{e}*}$, $\Delta I_{qs}^{\hat{e}*}$, and β_q, while desired dc current is injected simultaneously. By applying (15) to (22), $\Delta T_{e,\omega e}$ can be expressed as

$$\begin{aligned}\Delta T_{e,\omega_e} = \frac{3P}{4}\Big(&\Delta I_{qs}^{\hat{e}*}L_m I_{ds}^{\hat{e}*}\cos(\hat{\theta}_e-\beta_q) - \Delta I_{ds}^{\hat{e}*}MI_{ds}^{\hat{e}*}\cos(\hat{\theta}_e+\theta_M)\\ &-\Delta I_{qs}^{\hat{e}*}MI_{qs}^{*}\cos(\hat{\theta}_e-\beta_q+\theta_M) + \Delta I_{ds}^{\hat{e}*}NI_{qs}^{\hat{e}*}\cos(\hat{\theta}_e-\theta_N)\\ &-\Delta I_{qs}^{\hat{e}*}NI_{ds}^{\hat{e}*}\cos(\hat{\theta}_e-\beta_q-\theta_N)\Big). \quad (27)\end{aligned}$$

Since $\Delta T_{e,\omega e}$ is a linear combination of $\cos(\hat{\theta}_e)$ and $\sin(\hat{\theta}_e)$, $\Delta T_{e,\omega e}$ and $\frac{d}{d\hat{\theta}_e}\Delta T_{e,\omega e}$ cannot be zero at the same time for any $\hat{\theta}_e$ except when $\Delta T_{e,\omega e}=0$ for all $\hat{\theta}_e$. Therefore, $\Delta T_{e,\omega e}$ can be nullified for all $\hat{\theta}_e$, if and only if the following equations are satisfied.

$$\begin{aligned}\left|\Delta T_{e,\omega_e}|_{\text{conven.1}}\right| &= \frac{3P}{4}I_{DC\,Inj}^{\ *}\sqrt{\left(\left(N+M\sin(\theta_{M+N})\right)I_{qs}^{\hat{e}*} - M\cos(\theta_{M+N})I_{ds}^{\hat{e}*}\right)^2 + \left(M\cos(\theta_{M+N})I_{qs}^{\hat{e}*} - \left(L_m+N-M\sin(\theta_{M+N})\right)I_{ds}^{\hat{e}*}\right)^2}\\ &\approx \frac{3P}{4}I_{DC\,Inj}^{\ *}\sqrt{\left(\left(N+M\right)I_{qs}^{\hat{e}*}\right)^2 + \left(\left(L_m+N-M\right)I_{ds}^{\hat{e}*}\right)^2}. \quad (24)\end{aligned}$$

$$\left|\Delta T_{e,\omega_e}|_{\text{conven.2}}\right| = \frac{3P}{4}2I_{DC\,Inj}^{\ *}\sqrt{\left(NI_{qs}^{\hat{e}*} - MI_{ds}^{\hat{e}*}\cos(\theta_{M+N})\right)^2 + \left(MI_{ds}^{\hat{e}*}\sin(\theta_{M+N})\right)^2} \approx \frac{3P}{4}2I_{DC\,Inj}^{\ *}\sqrt{\left(NI_{qs}^{\hat{e}*}\right)^2 + \left(MI_{ds}^{\hat{e}*}\right)^2}. \quad (25)$$

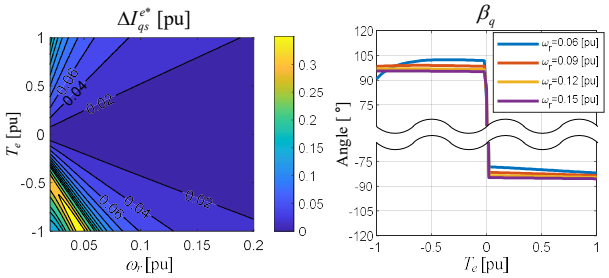

(a) (b)

Fig. 7. (a) $\Delta I_{qs}^{\hat{e}^*}$ and (b) β_q in the proposed method when $\Delta I_{ds}^{\hat{e}^*} = 0.2\,\text{pu}$.

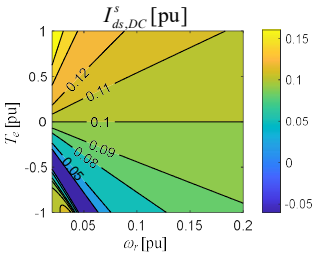

Fig. 8. Injected dc current when $\Delta I_{ds}^{\hat{e}^*} = 0.2\,\text{pu}$.

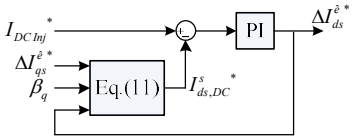

Fig. 9. dc current controller.

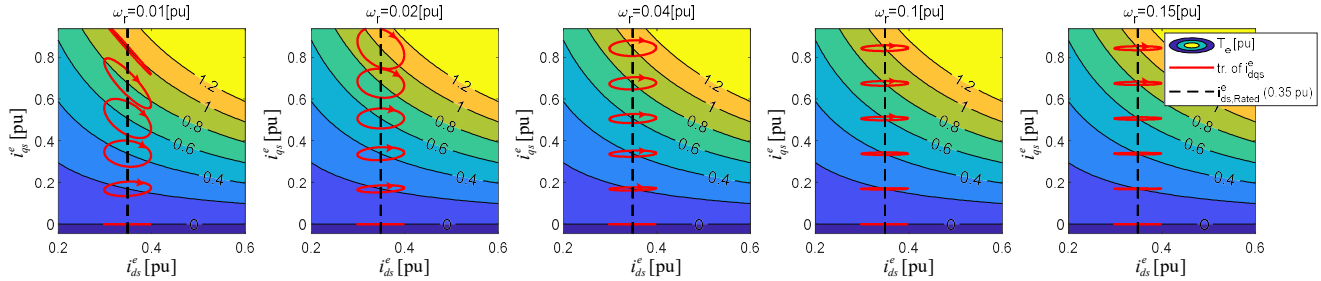

(a) (b) (c) (d) (e)

Fig. 10. Injected current trajectory (tr.) according to speed and load conditions. (a) ω_r=0.01 pu. (b) ω_r=0.02 pu. (c) ω_r=0.04 pu. (d) ω_r=0.1 pu. (e) ω_r=0.15 pu.

$$\Delta T_{e,\omega_e}\left(\beta_q\right) = 0\,. \tag{28}$$

$$\frac{d}{d\hat{\theta}_e}\Delta T_{e,\omega_e}\left(\beta_q\right) = 0\,. \tag{29}$$

By solving (28) and (29), $\Delta I_{qs}^{\hat{e}^*}$ and β_q nullifying the torque ripple for a $\Delta I_{ds}^{\hat{e}^*}$ can be obtained as follows:

$$\beta_q = \theta_N + \text{atan}\left(\frac{qa - qb\cos\left(\theta_{M+N}\right) + pb\sin\left(\theta_{M+N}\right)}{pa - qb\sin\left(\theta_{M+N}\right) - pb\cos\left(\theta_{M+N}\right)}\right) \tag{30}$$

and

$$\Delta I_{qs}^{\hat{e}^*} = -\frac{a}{p}\cos\left(\beta_q - \theta_N\right) + \frac{b}{p}\cos\left(\beta_q + \theta_M\right) \tag{31}$$

where

$$a = \Delta I_{ds}^{\hat{e}^*} N I_{qs}^{\hat{e}^*}\,. \tag{32}$$

$$b = \Delta I_{ds}^{\hat{e}^*} M I_{ds}^{\hat{e}^*}\,. \tag{33}$$

$$p = L_m I_{ds}^{\hat{e}^*} - N I_{ds}^{\hat{e}^*}\cos\left(\theta_N\right) - M I_{qs}^{\hat{e}^*}\cos\left(\theta_M\right). \tag{34}$$

$$q = N I_{ds}^{\hat{e}^*}\sin(\theta_N) - M I_{qs}^{\hat{e}^*}\sin(\theta_M)\,. \tag{35}$$

$\Delta I_{qs}^{\hat{e}^*}$ and β_q obtained from (30) and (31) for the IM under study are depicted in Fig. 7. $\Delta I_{ds}^{\hat{e}^*}$ is set to 20% of the rated current. In Fig. 7(a), $\Delta I_{qs}^{\hat{e}^*}$ is close to null at no load and in the high-speed condition. In Fig. 7(b), β_q is close to -90° for motoring mode, and 90° for regenerating mode regardless of the operating speed above 5% of the rated speed.

By substituting $\Delta I_{qs}^{\hat{e}^*}$ and β_q for (11), the injected dc current, $I_{ds,DC}^{s}$, can be calculated as shown in Fig. 8. Observing Fig. 7 and Fig. 8, followings can be figured out.

1) $I_{ds,DC}^{s}$ is reduced in the regenerating mode if $\Delta I_{ds}^{\hat{e}^*}$ is set to constant, and it increases in the motoring mode.

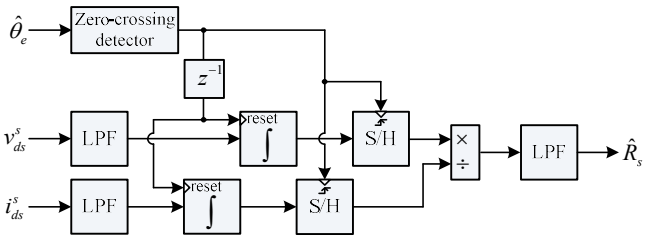

Fig. 11. Block diagram of dc signal extraction method.

2) Most of the injected dc current is on *d*-axis at the stationary reference frame, since $\cos(\beta_q) \approx 0$.

Therefore, to keep $I_{ds,DC}^{s}$ constant, $\Delta I_{ds}^{\hat{e}^*}$ should be changed according to speed and load conditions. To achieve constant $I_{ds,DC}^{s}$, a simple dc current controller can be designed as shown in Fig. 9. It calculates the injected dc current and adjusts $\Delta I_{ds}^{\hat{e}^*}$ to obtain the desired magnitude of dc current to be injected.

Fig. 10 depicts the trajectories of injected current on the synchronous reference frame for various speed and load conditions. In the high-speed region, the current trajectory coincides with that of Fig. 2(b) which does not inject *q*-axis current. On the contrary, the trajectory minimizing the torque ripple converges to the tangent line of the constant torque loci in the very low-speed region, as shown in Fig. 10(a).

D. DC Signal Extraction Method in the Low-Speed Region

Another obstacle to dc injection in the low-speed region is dc signal extraction. Most existing dc signal extraction methods are constructed with IIR low-pass and notch filters under the assumption that dc signal and operating frequency are far enough in the frequency band. However, it is hard to segregate

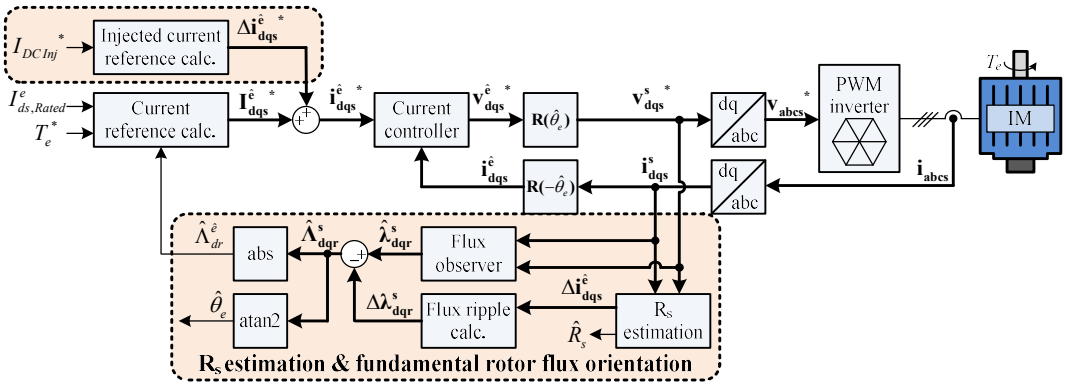

Fig. 12. Block diagram of proposed method.

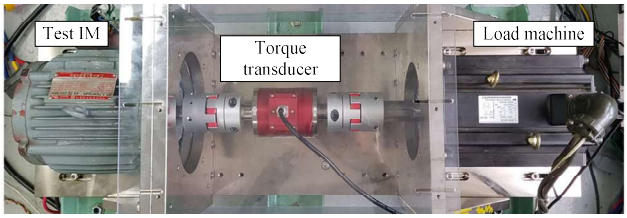

Fig. 13. Experimental setup.

the operating frequency and dc signal with linear filters in the low-speed region. Therefore, to extract dc component from phase current and voltage reference, this paper proposes a nonlinear dc extraction method using an average filter reset at every rotation period.

Fig. 11 shows the block diagram of the proposed dc signal extraction method. The key part consists of two simple blocks; an average filter and a sample and holder. First, every rotation period is known from $\hat{\theta}_e$. For every rotation period, the average filter integrates the current and voltage values, and they are sampled by the sample and holder. The estimated stator resistance, $\hat{R}_s$, can be obtained by dividing sampled voltage and current.

It is noticeable that an error in the rotation period would deteriorate the performance of the proposed extraction method. Therefore, FRFO is essential to avoid fluctuation in measuring the rotational period of IM. Besides, a low-pass filter is added before the integration to attenuate the effect of non-dc components which would be at the operating and 2nd harmonic frequency.

IV. Simulation & Experimental Results

A. Implementation

Fig. 12 shows the block diagram of the proposed dc injection method on FRFO. The sensorless flux observer is constructed by the method in [18], which estimates the instantaneous rotor flux on the stationary frame, $\hat{\boldsymbol{\lambda}}^{s}_{dqr}$. The flux ripple due to injected current in (30) and (31), $\Delta\boldsymbol{\lambda}^{s}_{dqr}{}^{*}$, is calculated. The fundamental rotor flux, $\hat{\boldsymbol{\Lambda}}^{s}_{dqr}$, is obtained by subtracting $\Delta\boldsymbol{\lambda}^{s}_{dqr}{}^{*}$ from $\hat{\boldsymbol{\lambda}}^{s}_{dqr}$.

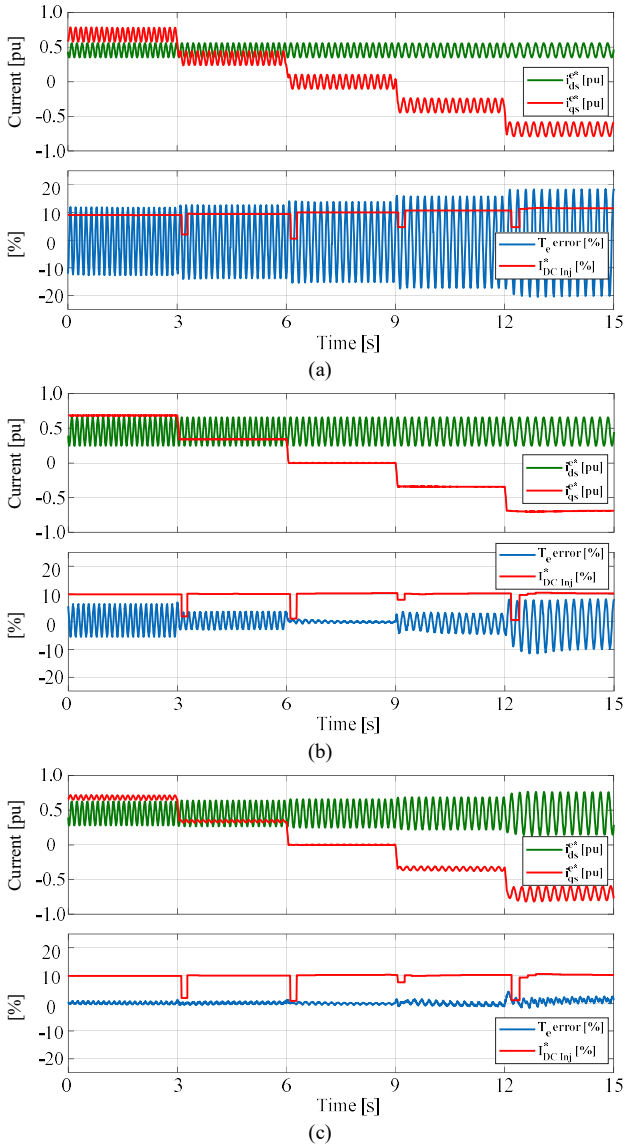

Fig. 14. dc current injection at ω_r=0.1pu (Simulation results).
(a) Conventional method 1. (b) Conventional method 2. (c) Proposed method.

The algorithm of Fig. 12 is implemented on simulation and through the experimental setup. The current control bandwidth is set to 300 Hz to regulate the injected current without delay. For the verification of the proposed method, torque ripples are

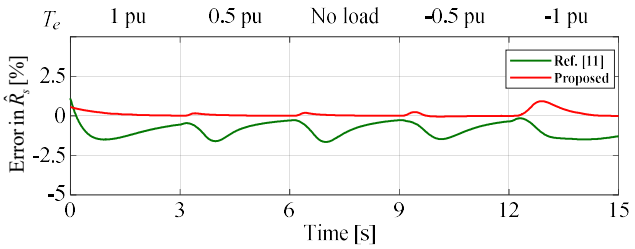

Fig. 15. R_s estimation at ω_r=0.1pu (Simulation results).

compared in conventional methods and proposed method. IM in TABLE I, shown in Fig. 13, is used for the experimental verification. In the experiments, a torque sensor is used to measure the output torque ripple. The magnitude of injected dc current is set to 10% of rated current in all methods.

B. Simulation Results

Fig. 14 shows the simulation results at 10% of rated speed. Load torque is varied from -1pu to 1pu, injecting dc current simultaneously. In Fig. 14(a), the torque ripple is considerable regardless of load condition. In Fig. 14(b), since the q-axis current injection is removed, the torque ripple in light load condition is reduced near to null. However, the torque ripple appears in loaded condition and the magnitude of torque ripple increases to around 9% of rated torque in the full regenerative load. These results correspond to Fig. 6. However, with the proposed method, the torque ripple is reduced conspicuously regardless of the same magnitude of the injected dc current to conventional method 2. As discussed in chapter III.A, remaining torque ripple with 2nd order harmonic, $\Delta T_{e,2\omega e}$, is much smaller than $\Delta T_{e,\omega e}$.

R_s estimation error under load changes is depicted in Fig. 15 to verify the effectiveness of the proposed dc extraction method. The extraction method in [11], which is based on the frequency-based linear filter, is implemented for the comparison. The proposed dc injection method in Fig. 14(c) is applied to both extraction methods. For the fair comparison, the bandwidth of the low-pass filters has been set to 0.25 Hz for both cases in calculating $\hat{R}_s$. In Fig. 15, the proposed extraction method shows better dynamics under load change than the conventional linear filter, which has severe transient errors.

C. Experimental Results

Fig. 16 shows the experimental results corresponding to the simulation results. The magnitude of injected dc current is well-regulated around 10% of rated current in all three methods, and the magnitudes of torque ripple are very similar to those of the simulation results. The maximum magnitude of torque ripple in the proposed method is around 3% of rated torque. The increase of torque ripple compared to simulation results could come from parameter mismatch and other torque ripple sources such as cogging torque of the load machine.

The performance of R_s estimation is verified in Fig. 17. The motor speed is maintained at 10% of the rated speed in the test process. For the first 300s, IM under test applies the full motoring load without R_s estimation. Since the error in $\hat{R}_s$

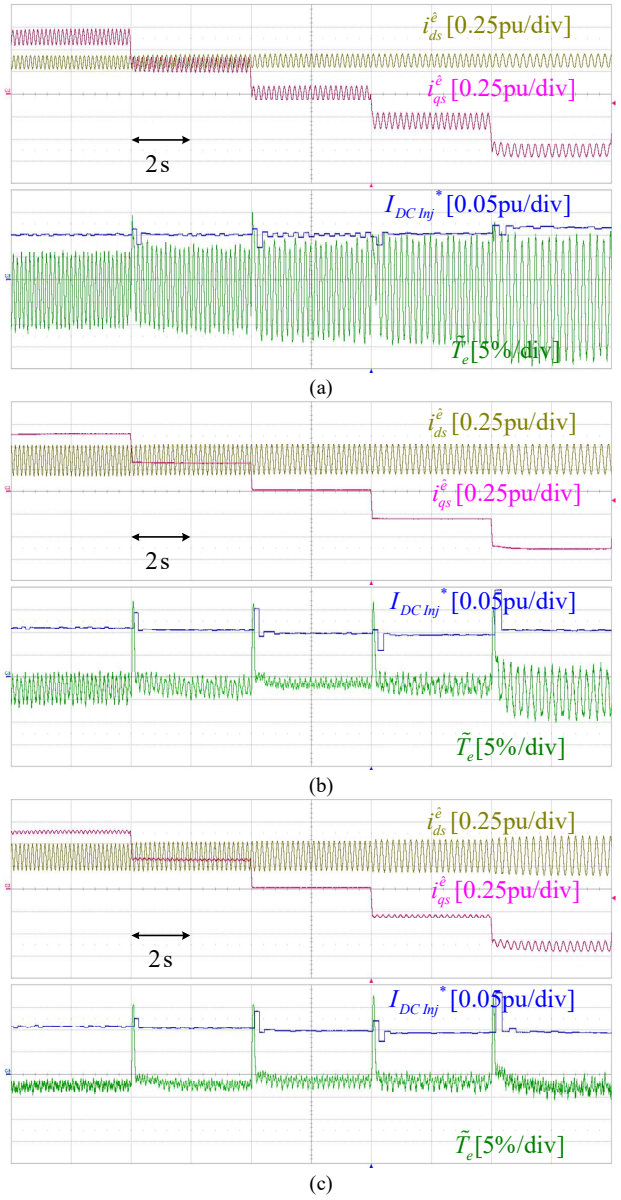

Fig. 16. dc current injection at ω_r=0.1pu (Experimental results).
(a) Conventional method 1. (b) Conventional method 2. (c) Proposed method.

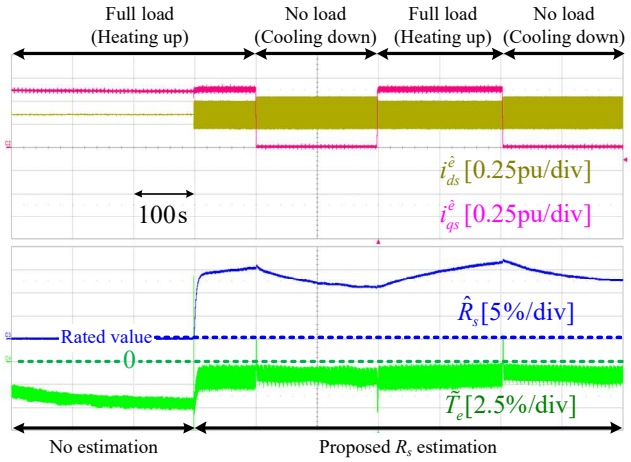

Fig. 17. Proposed R_s estimation under load torque variation (Long term).

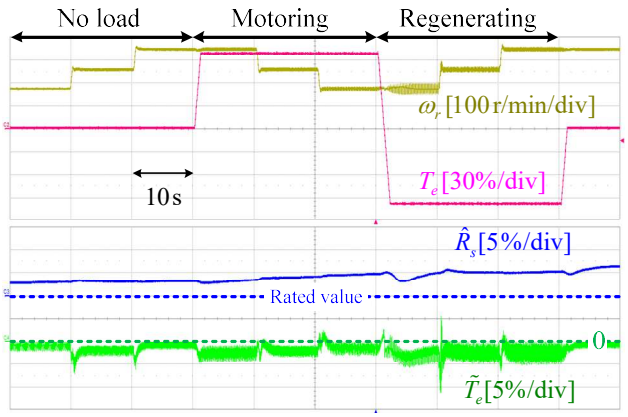

Fig. 18. Proposed R_s estimation at various operating conditions.

directly deteriorates the torque accuracy, the torque error increases up to 5% of the rated torque as the temperature rise due to the full load operation. From 300s, the proposed method starts to estimate R_s, and the average torque error is reduced below 2.5% of the rated torque. From the results, it can be said that R_s estimation works properly following temperature fluctuation due to repeated no-load and full-load conditions. The torque error is well-regulated under 2.5% regardless of the temperature rise and the operating conditions in the sensorless control mode.

In Fig. 18, the performance of R_s estimation at various operating conditions in sensorless control is depicted. IM under test applies null torque, full motoring load, and full regenerating load and the motor speed is changed to 10%, 15% and 20% of the rated speed for each load condition. For the whole test process of 100s, the magnitude of torque ripple is well-regulated within 2.5% of rated torque, thanks to the proposed method. The estimated R_s slightly increases from 1.03 times of the rated value to 1.06 times due to the resistive loss of the stator winding.

V. Conclusion

This paper proposes a torque ripple reduction method and a dc signal extraction method in dc current injection in the low-speed region in sensorless control of induction motor. First, the flux ripple in arbitrary dc and 2nd harmonic current injection has been analyzed. Based on the analysis, the current reference, which nullifies torque fluctuation, is calculated. For the extraction of dc voltage and current information, angle based averaging filter has been proposed. In the proposed method, the perturbation issue in the synchronous speed of rotor flux orientation is avoided by applying fundamental rotor flux orientation. The applicability of the proposed method is verified by simulation and experimental results. Thanks to the proposed method, the stator resistance, which is the most crucial parameter to the stability and torque accuracy of sensorless control of the induction motor at low speed, is accurately estimated. And, at overall load torque conditions in the low-speed region, the torque control accuracy has been improved from 5% error bound to 2.5% error bound still keeping torque ripple under negligible magnitude.

Appendix

Flux Ripple due to Current Injection

Applying (13) to (12), the following equations can be deduced.

$$\mathbf{S}\begin{bmatrix}\Delta\Lambda^{\hat{e}}_{dr,\sin}\\ \Delta\Lambda^{\hat{e}}_{qr,\sin}\end{bmatrix} = L_m\begin{bmatrix}\Delta I^{\hat{e}\,*}_{ds,\cos}\\ \Delta I^{\hat{e}\,*}_{qs,\cos}\end{bmatrix} - \mathbf{T}\begin{bmatrix}\Delta\Lambda^{\hat{e}}_{dr,\cos}\\ \Delta\Lambda^{\hat{e}}_{qr,\cos}\end{bmatrix} \tag{36}$$

and

$$-\mathbf{S}\begin{bmatrix}\Delta\Lambda^{\hat{e}}_{dr,\cos}\\ \Delta\Lambda^{\hat{e}}_{qr,\cos}\end{bmatrix} = L_m\begin{bmatrix}0\\ \Delta I^{\hat{e}\,*}_{qs,\sin}\end{bmatrix} - \mathbf{T}\begin{bmatrix}\Delta\Lambda^{\hat{e}}_{dr,\sin}\\ \Delta\Lambda^{\hat{e}}_{qr,\sin}\end{bmatrix} \tag{37}$$

where

$$\mathbf{S} = \begin{bmatrix} f & 0\\ 0 & f\end{bmatrix}. \tag{38}$$

$$\mathbf{T} = \begin{bmatrix} 1 & -g\\ g & 1\end{bmatrix}. \tag{39}$$

Eq. (36) and (37) can be rewritten as follows:

$$\mathbf{P}\begin{bmatrix}\Delta\Lambda^{\hat{e}}_{dr,\cos}\\ \Delta\Lambda^{\hat{e}}_{qr,\cos}\\ \Delta\Lambda^{\hat{e}}_{dr,\sin}\\ \Delta\Lambda^{\hat{e}}_{qr,\sin}\end{bmatrix} = L_m\begin{bmatrix}\Delta I^{\hat{e}\,*}_{ds,\cos}\\ \Delta I^{\hat{e}\,*}_{qs,\cos}\\ 0\\ \Delta I^{\hat{e}\,*}_{qs,\sin}\end{bmatrix} \tag{40}$$

where

$$\mathbf{P} = \begin{bmatrix}\mathbf{T} & \mathbf{S}\\ -\mathbf{S} & \mathbf{T}\end{bmatrix}. \tag{41}$$

Therefore, multiplying $\mathbf{P}^{-1}$, the flux ripple can be calculated as follows:

$$\begin{bmatrix}\Delta\Lambda^{\hat{e}}_{dr,\cos}\\ \Delta\Lambda^{\hat{e}}_{qr,\cos}\\ \Delta\Lambda^{\hat{e}}_{dr,\sin}\\ \Delta\Lambda^{\hat{e}}_{qr,\sin}\end{bmatrix} = \frac{L_m}{\det(\mathbf{P})}\begin{bmatrix} a_1 & a_2 & -a_3 & a_4\\ -a_2 & a_1 & -a_4 & -a_3\\ a_3 & -a_4 & a_1 & a_2\\ a_4 & a_3 & -a_2 & a_1\end{bmatrix}\begin{bmatrix}\Delta I^{\hat{e}\,*}_{ds,\cos}\\ \Delta I^{\hat{e}\,*}_{qs,\cos}\\ 0\\ \Delta I^{\hat{e}\,*}_{qs,\sin}\end{bmatrix} \tag{42}$$

where

$$a_1 = f^2 + g^2 + 1. \tag{43}$$

$$a_2 = \left(f^2 - g^2 - 1\right)g. \tag{44}$$

$$a_3 = \left(f^2 - g^2 + 1\right)f. \tag{45}$$

$$a_4 = 2fg. \tag{46}$$

In (42), det(**P**) can be calculated as follows:

$$\begin{aligned}\det(\mathbf{P}) &= \left(f^2 - g^2 + 1\right)^2 + 4g^2\\ &= \left(-f^2 + g^2 + 1\right)^2 + 4f^2\\ &= \left(f^2 + g^2 + 1\right)^2 + 4f^2g^2.\end{aligned} \tag{47}$$

Observing (42) and (47), M, N, θ_M, and θ_N can be deduced as follows:

$$M = L_m \sqrt{\frac{a_2^{\,2} + a_4^{\,2}}{\det(\mathbf{P})^2}} = L_m \frac{g}{\sqrt{\det(\mathbf{P})}}. \quad (48)$$

$$N = L_m \sqrt{\frac{a_1^{\,2} + a_3^{\,2}}{\det(\mathbf{P})^2}} = L_m \frac{1+f^2}{\sqrt{\det(\mathbf{P})}}. \quad (49)$$

$$\tan\theta_M = \frac{a_4}{a_2} = \frac{2f}{f^2 - g^2 - 1}. \quad (50)$$

$$\tan\theta_N = \frac{a_3}{a_1} = f\frac{f^2 - g^2 + 1}{f^2 + g^2 + 1}. \quad (51)$$

ACKNOWLEDGMENT

This work was supported by the Seoul National University Electric Power Research Institute, by the Brain Korea 21 Plus Project in 2018, granted financial resource from the Ministry of Trade, Industry & Energy, Republic of Korea, and by Yaskawa Electric Co., Japan.

REFERENCES

[1] Jang-Hwan Kim, Jong-Woo Choi and Seung-Ki Sul, "Novel rotor-flux observer using observer characteristic function in complex vector space for field-oriented induction motor drives," in *IEEE Transactions on Industry Applications*, vol. 38, no. 5, pp. 1334-1343, Sept.-Oct. 2002.

[2] L. Harnefors and M. Hinkkanen, "Stabilization Methods for Sensorless Induction Motor Drives−A Survey," in *IEEE Journal of Emerging and Selected Topics in Power Electronics*, vol. 2, no. 2, pp. 132-142, June 2014.

[3] V. Vasic, S. N. Vukosavic and E. Levi, "A stator resistance estimation scheme for speed sensorless rotor flux oriented induction motor drives," in *IEEE Transactions on Energy Conversion*, vol. 18, no. 4, pp. 476-483, Dec. 2003.

[4] M. S. Zaky, "Stability Analysis of Speed and Stator Resistance Estimators for Sensorless Induction Motor Drives," in *IEEE Transactions on Industrial Electronics*, vol. 59, no. 2, pp. 858-870, Feb. 2012.

[5] M. Hinkkanen, L. Harnefors and J. Luomi, "Reduced-Order Flux Observers With Stator-Resistance Adaptation for Speed-Sensorless Induction Motor Drives," in *IEEE Transactions on Power Electronics*, vol. 25, no. 5, pp. 1173-1183, May 2010.

[6] S. D. Wilson, G. W. Jewell and P. G. Stewart, "Resistance estimation for temperature determination in PMSMs through signal injection," *IEEE International Conference on Electric Machines and Drives, 2005.*, San Antonio, TX, 2005, pp. 735-740.

[7] L. He, J. Restrepo, S. Cheng, R. G. Harley and T. G. Habetler, "An improved DC-signal-injection method with active torque-ripple mitigation for thermal monitoring of field-oriented-controlled induction motors," *2015 IEEE Energy Conversion Congress and Exposition (ECCE)*, Montreal, QC, 2015, pp. 4447-4454.

[8] F. Baneira, J. Doval-Gandoy, A. G. Yepes and O. López, "DC-Current Injection With Minimum Torque Ripple in Interior Permanent-Magnet Synchronous Motors," in *IEEE Transactions on Power Electronics*, vol. 35, no. 2, pp. 1176-1181, Feb. 2020.

[9] F. Baneira, A. G. Yepes, Ó. López and J. Doval-Gandoy, "Estimation Method of Stator Winding Temperature for Dual Three-Phase Machines Based on DC-Signal Injection," in *IEEE Transactions on Power Electronics*, vol. 31, no. 7, pp. 5141-5148, July 2016.

[10] P. R. Matić, M. A. Gecić, D. M. Lekić and D. P. Marčetić, "Thermal Protection of Vector-Controlled IM Drive Based on DC Current Injection," in *IEEE Transactions on Industrial Electronics*, vol. 62, no. 4, pp. 2082-2089, April 2015.

[11] S. Cheng, Y. Du, J. A. Restrepo, P. Zhang and T. G. Habetler, "A Nonintrusive Thermal Monitoring Method for Induction Motors Fed by Closed-Loop Inverter Drives," in *IEEE Transactions on Power Electronics*, vol. 27, no. 9, pp. 4122-4131, Sept. 2012.

[12] M. O. Sonnaillon, G. Bisheimer, C. D. Angelo and G. O. García, "Online Sensorless Induction Motor Temperature Monitoring," in *IEEE Transactions on Energy Conversion*, vol. 25, no. 2, pp. 273-280, June 2010.

[13] F. Baneira, L. Asiminoaei, J. Doval-Gandoy, H. A. M. Delpino, A. G. Yepes and J. Godbersen, "Estimation Method of Stator Winding Resistance for Induction Motor Drives Based on DC-Signal Injection Suitable for Low Inertia," in *IEEE Transactions on Power Electronics*, vol. 34, no. 6, pp. 5646-5654, June 2019.

[14] J. Faiz and M. B. B. Sharifian, "Different techniques for real time estimation of an induction motor rotor resistance in sensorless direct torque control for electric vehicle," in *IEEE Transactions on Energy Conversion*, vol. 16, no. 1, pp. 104-109, March 2001.

[15] P. Vaclavek and P. Blaha, "Lyapunov-function-based flux and speed observer for AC induction motor sensorless control and parameters estimation," in *IEEE Transactions on Industrial Electronics*, vol. 53, no. 1, pp. 138-145, Feb. 2006.

[16] M. Shin and D. Hyun, "Online Identification of Stator Transient Inductance in Rotor-Flux-Oriented Induction Motor Drive," in *IEEE Transactions on Industrial Electronics*, vol. 54, no. 4, pp. 2018-2023, Aug. 2007.

[17] J. Yoo, J. Lee, S. Sul and N. A. Baloch, "Torque Ripple Reduction in Stator Resistance Estimation using DC Current Injection for Induction Motor Sensorless Drives," *2019 IEEE Energy Conversion Congress and Exposition (ECCE)*, Baltimore, MD, USA, 2019, pp. 7057-7063.

[18] S. Suwankawin and S. Sangwongwanich, "A speed-sensorless IM drive with decoupling control and stability analysis of speed estimation," in *IEEE Transactions on Industrial Electronics*, vol. 49, no. 2, pp. 444-455, April 2002.